

Article

Low-Noise Airfoils for Turbomachinery Applications: Two Examples of Optimization [†]

Nicola Casari ^{1,2}, Ettore Fadiga ¹, Stefano Oliani ¹, Mattia Piovan ^{1,*}, Michele Pinelli ¹ and Alessio Suman ¹ 

¹ Department of Engineering, University of Ferrara, Via Giuseppe Saragat 1, 44122 Ferrara, Italy; n.casari@toffeeam.co.uk (N.C.); etttore.fadiga@unife.it (E.F.); stefano.oliani@unife.it (S.O.); michele.pinelli@unife.it (M.P.); alessio.suman@unife.it (A.S.)

² TOffeAM Ltd., 16-16A Baldwin's Gardens, The Record Hall, London EC1N 7RJ, UK

* Correspondence: mattia.piovan@unife.it

[†] This paper is an extended version of our paper published in Proceedings of the 15th European Turbomachinery Conference, Budapest, Hungary, 24–28 April 2023.

Abstract: Automotive fans, small wind turbines, and manned and unmanned aerial vehicles (MAVs/UAVs) are just a few examples in which noise generated by the flow's interaction with aerodynamic surfaces is a major concern. The current work shows the potential of a new airfoil shape to minimize noise generation, maintaining a high lift-to-drag ratio in a prescribed Reynolds regime. This investigation uses a multifidelity approach: a low-fidelity semiempirical model is exploited to evaluate the sound pressure level (SPL). Fast evaluation of a low-cost function enables the computation of a large range of possible profiles, and accuracy is added to the low-fidelity response surface with high-fidelity CFD data. The constraint of maintaining a predefined range of the lift coefficient and lift-to-drag ratio ensures the possibility of using this profile in usual design procedures.

Keywords: self-noise; noise suppression; aeroacoustics; multifidelity optimization



Citation: Casari, N.; Fadiga, E.; Oliani, S.; Piovan, M.; Pinelli, M.; Suman, A. Low-Noise Airfoils for Turbomachinery Applications: Two Examples of Optimization. *Int. J. Turbomach. Propuls. Power* **2024**, *9*, 9. <https://doi.org/10.3390/ijtp9010009>

Academic Editor: Antoine Dazin

Received: 8 August 2023

Revised: 19 January 2024

Accepted: 5 February 2024

Published: 2 March 2024



Copyright: © 2024 by the authors. Licensee MDPI, Basel, Switzerland. This article is an open access article distributed under the terms and conditions of the Creative Commons Attribution (CC BY-NC-ND) license (<https://creativecommons.org/licenses/by-nc-nd/4.0/>).

1. Introduction

Due to an ecological transition, Internal Combustion Engine (ICE) vehicles are being replaced by electric vehicles. As is well known, electrical motors are silent compared with ICEs. Therefore, the relevance of other noise sources increases. Among others, the cooling fan represents a major noise emitter [1], and it is therefore of interest for manufacturers to improve its performance, including the perceived sound.

Another effect of the ecological transition is the passage from fossil to renewable energy generation. One of the most used technologies for such a scope is wind turbines. However, the use of this type of machine in the proximity of human habitats is limited by noise emission, as described by [2]. This is specifically important for the urban integration of small-scale wind turbines.

These two cited applications are just examples of the importance of correct noise prediction and suppression: noise generation is increasingly considered as a factor hindering new technology uptake. In order to tackle this problem, it should be noted that in both issues, one of the main noise sources is aerodynamic noise, i.e., the sound emitted due to the flow's interaction with airfoils and aerodynamic surfaces. In the literature, a limited number of experimental tests and numerical results are available, especially in the low-Reynolds regime, to predict both the aerodynamic and noise performances of an airfoil. This work is intended to study the effects of airfoil shape on noise generation, keeping in mind, as the final application, an axial fan for a cooling system. However, this choice does not limit the generality of the results.

The study proposed here focuses on what is typically referred to as self-noise, which is the noise generated by blades operating in a clean, undisturbed flow [3]; thus, it represents the minimum fan noise that is emitted without installation effects. The interaction between

the blade's turbulent boundary layer and a geometrical discontinuity, like the bluntness at the trailing edge, constitutes one of the most important noise generation mechanisms, known as trailing-edge noise. Moreover, leakage and tip vortex flows can constitute a fundamental mechanism for fan noise [4]. Aeroacoustics researchers are focusing on two different strategies to reduce airfoil self-noise. The first one consists of designing low-noise aerodynamic profiles [5], while the second one introduces leading and/or trailing-edge serrations on the blades. For example, specific airfoil families have been designed for wind turbines to replace traditional airfoils, such as the four-digit NACA series. Ad hoc geometries are used to have a high lift-to-drag ratio, high resistance to wear, and low noise emission. In the few last years, 3D spanwise features have been applied to blades to reduce the amount of noise generated by a straight trailing edge; the lift-to-drag ratio of this type of solution depends on both the angle of attack and Reynolds number [6]. For this reason, there is not a general rule to develop the best 3D feature.

Historically, the coupled acoustic–aerodynamic performances of an airfoil are studied using analytical or semiempirical approaches and experimentally. Recently, CFD simulations were used with outstanding results to predict the aerodynamic performances of a turbomachine. A very limited number of fan blade shape optimizations for noise reduction are available in the literature. One of them is [7], in which BEM and the Ffowcs Williams–Hawkings analogy [8] are used to compute the fan acoustics, and the geometry optimization of the blade is carried out by a genetic algorithm.

This work presents an airfoil shape optimization starting from a NACA 64618, using semiempirical (low-fidelity) and CFD (high-fidelity) approaches. The authors aim to show the airfoil shape that gives the best acoustics response in a specific frequency range at a fixed lift coefficient and lift-to-drag ratio. The low-noise profile obtained with the optimization process can directly replace the ones used for fan design.

2. Methodology

Different methodologies can be used to determine the correct estimation of the self-noise generated to design a silent airfoil. In particular, different tools require different levels of accuracy and computational time. Fast and low-fidelity tools might be preferred over slower but higher-fidelity tools in the initial design phase. Within this work, two different computational methods are employed, representing the two different levels of accuracy: a semiempirical approach and a CFD solution. By low fidelity, the authors mean an empirical/semiempirical model or a model that uses a less general method than the high-fidelity one to solve a problem. In the following, both methodologies are presented.

The low-fidelity approach chosen is named the BPM method (from the authors' first names, Brooks, Pope, and Marcolini) [9]. This method was cross-checked with experimental data. After the validation phase, the BPM method was used in a Simplicial Homology Global Optimizer (SHGO) to determine the airfoil shape with the lowest Overall Sound Pressure Level (OSPL), (1) with A-weighted correction in the frequency range between 100 and 5000 Hz. The A-weighted correction was applied to the OSPL to approximate adequate human hearing sensation.

$$SPL_{overall} = 10 \log_{10} \left(\frac{\sqrt{\sum p^2}}{p_{ref}} \right)^2 \quad (1)$$

In the first phase of the work, the NACA 64618 airfoil was tested in the high-Reynolds number regime ($1.8 \cdot 10^6$) to validate both low- and high-fidelity tools with the experimental data taken from [10]. The chord length for the NACA generation was 0.6m and the span is 1.62 m. The inflow angle of attack was -0.258° , corresponding to a lift coefficient of 0.5. After this step, the same airfoil was tested in a low-Reynolds number case ($2 \cdot 10^5$) to cross-validate the used instruments in the low-Reynolds regime. In the last part of the work, two geometrical optimizations were performed, the first one in the high-Reynolds regime and the second one in the low-Reynolds regime.

2.1. Low-Fidelity Approach

The semiempirical BPM model derives from the effort of correlating experimental tests on the NACA 0012 airfoil with different configurations (i.e., trip and TE bluntness) and flow conditions. The authors of [9] developed a correlation to quantify self-noise based on the Reynolds number and the angle of attack. To formulate such a scaling law, the authors decomposed the airfoil self-noise according to five different mechanisms: (i) Turbulent Boundary Layer–Trailing-Edge (TBL-TE) divided into the pressure side (TBL-PS) and suction side (TBL-SS); (ii) Separation stall (TBL-Sep); (iii) Laminar Boundary Layer Vortex-Shedding (Laminar); (iv) Tip vortex formation; and (v) Trailing-Edge Bluntness Vortex-Shedding. Due to the particular configuration chosen in this work, no tip noise is considered. Also, the (v) contribution was not included in the total SPL calculation due to the sharp TE. The formulation of the scaling laws was not reported here for brevity. The reader is referred to [9] for the formal description and to [11] for their implementation of the current framework.

The authors of the BPM model [9] also provided a correlation for the displacement thickness calculation, which was crucial for correctly predicting the generated noise. The correlation provided was validated on a NACA 0012 profile, and no guarantee was given on its applicability to other airfoils. To extend the generality of the model, the acoustic prediction was coupled with XFOIL [12]. An automatic procedure was beneficial in an optimization process since calculating the airfoil's parameters must be called several times. For this reason, the boundary layer parameters were calculated via XFOIL and used by the BPM model for noise prediction. The boundary layer thickness was unavailable within XFOIL; therefore, it was calculated from the displacement thickness δ^* . The boundary layer thickness δ was assumed to be equal to $\delta = 3\delta^*$; this is a commonly used approximation from the literature that also provided reasonable results in this application.

2.2. High-Fidelity Approach

The high-fidelity model, represented by a CFD solver, was used to verify the results of the low-fidelity approach related to the sharpened NACA 64618 profile (initial profile) and the optimized airfoil. The CFD solution was obtained with the usage of the open-source package OpenFOAM-v2206. To have a correct evaluation of the turbulence, fundamental for the proper prediction of the broadband noise and therefore, the SPL, a Large-Eddy Simulation (LES) was required. In OpenFOAM, different LES models were available. In this work, in order to return the correct wall behavior for wall-bounded flows, the Wall-Adapting Local Eddy viscosity (WALE) SubGrid Scale model from [13] was used. The solution was initialized with an unsteady RANS simulation obtained with a Langtry–Menter $k-\omega$ SST turbulence model developed by [14]. The transient simulation was carried out at a fixed time-step of $5 \mu\text{s}$ in order to maintain the maximum CFL around a value of 0.8. Regarding the numerical schemes, at least second-order discretization was used for the transient, turbulence, and velocity terms.

Figure 1 reports the overall set-up used for the numerical calculations. This set-up was selected to approximate the anechoic wind tunnel that was used by [10] for experimental testing. In the experimental set-up, there were Kevlar windows that enclosed the airfoil. To account for the effects of these windows, the upper and the lower walls of the fluid-dynamic domain were considered as no-slip walls. Regarding the mesh, a fully structured H-type grid was realized both on NACA 64618 and the optimal profile, with a 3D development span equal to $1/5$ of the chord. In proximity to the wall, the typical grid size for a Large-Eddy Simulation (LES) was imposed, where— $x^+ = 50$, $y^+ = 1.2$, and $z^+ = 25$. Moreover, the recommendations for a good aeroacoustic simulation described in [15] were applied. To check the quality of the mesh, the Celik index was used, [16]. In particular, this parameter was higher than 0.8 in the entire domain, indicating a satisfactory resolution of the mesh.

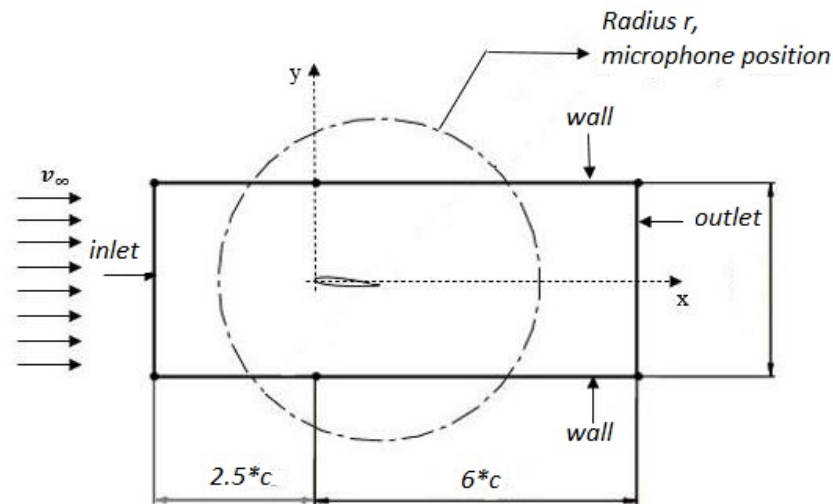


Figure 1. Representation of the numerical domain.

The official release of OpenFOAM-v2206 provides an acoustic tool based on the Curle analogy; this analogy was very limiting because it did not allow to account for surfaces in motion or to have permeable integral surfaces. For this reason, the libacoustics tools from [17], which implement the FWH analogy, were used to evaluate the acoustic pressure fluctuation. A permeable integration surface that encloses the airfoil was used in order to consider the volume of noise generated by the wake.

2.3. Optimization

XFOIL was used to assess the performance of the various shapes of the airfoil proposed by the optimizer. In fact, this tool contains a utility that enables modifying a base distribution of points, changing the position and maximum value of both camber and thickness. To better understand the airfoil's geometrical parameters changed by the optimizer, Figure 2 shows a sketch of an airfoil with geometrical features.

The base distribution chosen was the NACA 64618 airfoil. The following four different parameters were changed by the optimizer in the respective range referenced by the chord length: (i) position of camber 0.2–0.6, (ii) value of maximum camber 0.0–0.3, (iii) position of maximum thickness 0.1–0.5, and (iv) maximum thickness 0.1–0.5. The constraints have been imposed to limit the number of XFOIL calculations that do not converge. Within the optimization process, the best airfoil shape was determined by fixing both the lift coefficient and the lift-to-drag ratio, while the angle of attack was left free to vary.

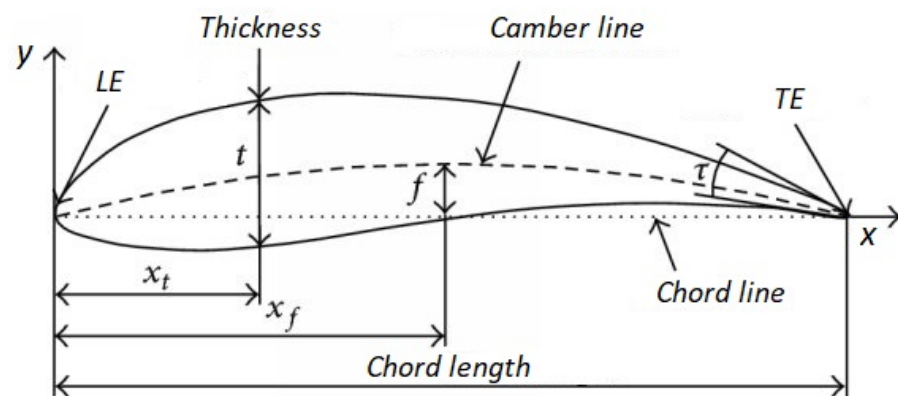


Figure 2. Airfoil geometry parameters. Image freely inspired by [18].

3. Results

In this section, the comparison between the BPM method, FWH analogy, and the experimental data for the validation case of NACA 64618 with a Reynolds number of $1.8 \cdot 10^6$ is shown. The experimental data were taken by [10]. In particular, the selected case had an angle of attack of -0.268° , corresponding to a lift coefficient of 0.5. The virtual microphone was placed at a distance of 0.42 m upstream of the TE and vertically at a distance of 1.62 m, as described by [10]. Once the Reynolds number was set, the optimization process started from the NACA 64618 airfoil, and by modifying both the position and the maximum camber and thickness values, the best geometries were found.

3.1. NACA 64618 Validation Case

The panel method implemented in XFOIL predicted a lift coefficient of 0.5 and a drag coefficient of 0.0057. Moreover, separation on both sides was predicted at 55 % of the chord length. These results were compared with those obtained from the 3D LES simulation, which provided a lift coefficient of 0.52 and a drag coefficient of 0.0061. The CFD analysis also confirmed the separation on the pressure and suction side. Figure 3, compares the airfoil surface's pressure coefficient, obtained with XFOIL and with CFD. There was a good match between the trends, and both methods predicted the same point of separation at 0.55^*c . The low-fidelity tool, however, predicted a lower pressure coefficient on the suction side.

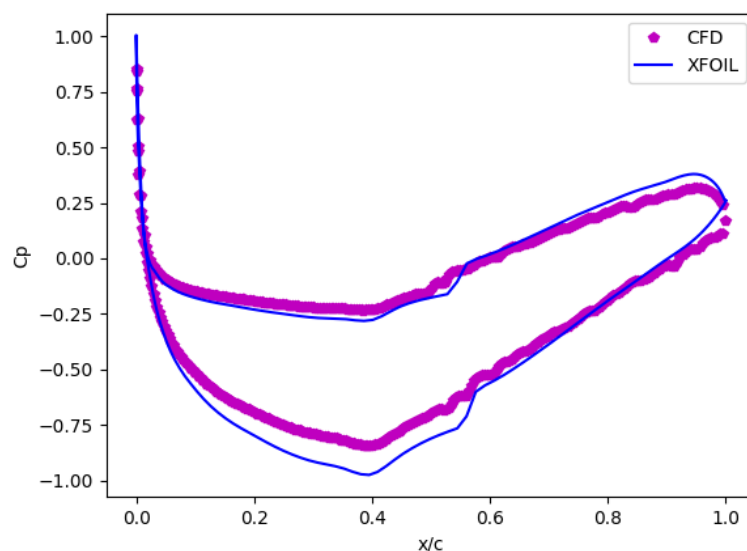


Figure 3. Pressure coefficient trend on the NACA 64618 airfoil.

Concerning the acoustics, the BPM model returns the frequency spectrum reported in Figure 4, and a corresponding OSPL calculated with Equation (1) of 62.5 dB_A was obtained. The peak of the SPL was 800 Hz, and it was due to the turbulent boundary layer on the suction side of the airfoil, while at the higher frequencies, the major contribution was due to the turbulent boundary layer on the pressure side. The laminar contribution and the separation provide negligible contributions in this case. The BPM results and the experimental data had the same trend, but the SPL values for the experimental data were about 5 dB lower. Figure 4 also reports the results obtained with the FWH analogy. The data were reported to the real airfoil span using the correlation taken by [19]. The trend obtained with the FWH analogy agreed with both experimental and BPM results, while the absolute value of the SPL away from the peak frequency was slightly higher than the BPM. Overall, a satisfactory agreement between experimental data, low-fidelity tools, and high-fidelity CFD was recorded for the case of aerodynamic and acoustics performances.

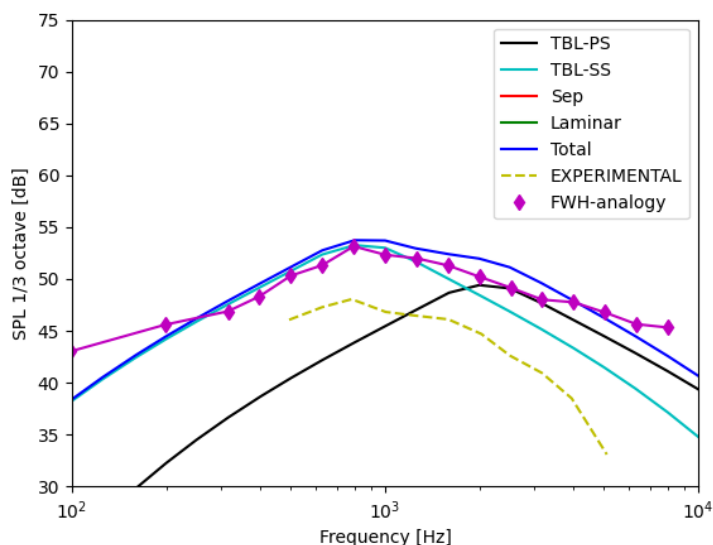


Figure 4. SPL 1/3 octave bands for the NACA 64618 validation case.

3.2. High-Reynolds Optimization

Initially, the airfoil geometry parameters were changed one by one to understand the relationship between the individual geometrical features and the acoustic emission. In the following, the NACA 64618 is taken as the baseline. Each parameter (i.e., thickness, the position of maximum thickness, maximum camber, and position of maximum camber) was then increased to a given quantity to assess the response in terms of the acoustic spectrum. The following conclusions were then found:

1. Thickness: Both the T-PS and the T-SS contribution had a higher value, and the maximum value was reached for a lower frequency.
2. Position of maximum thickness: Similar effects as the thickness contribution—increased noise emissions and shift towards lower frequencies. In this case, increasing the parameters translated into displacing the maximum thickness position towards the TE.
3. Maximum camber value: Both T-PS and T-SS contributions had a higher maximum value, but in this case, the frequencies at which these values are reached remain unchanged.
4. Position of maximum camber: The same effects as the maximum camber contribution.

Therefore, the pursuit of a silent airfoil will return a shape with a lower thickness distribution, with the maximum displacement toward the LE. The effect of the camber was an order of magnitude lower concerning the thickness contribution. After evaluating the single geometry effects, all the parameters were simultaneously changed by the SHGO optimizer to develop the airfoil shape that gives the lowest OSPL. The optimization process provided the following geometry parameters, based on chord length, for the silent airfoil: (i) position of maximum thickness— $0.30c$; (ii) maximum thickness— $0.1c$; (iii) camber value— $0.042c$; and (iv) position of maximum camber— $0.50c$. Figure 5 compares the optimal geometry and the initial one; from this, it is possible to notice how the new airfoil is more cambered and thinner than the original airfoil. These considerations confirm the conclusion described above.

The angle of attack that gave a lift coefficient of 0.5 with the low-fidelity tool is -1.310° , corresponding to a drag coefficient of 0.00514. The XFOIL software also predicted a little separation on both sides of the airfoil; in particular, the separation point on the pressure side was predicted at a distance of $0.42c$ from the leading edge, while the one on the suction side was predicted at a distance of $0.68c$. To validate the XFOIL results, a URANS simulation using the SST-LM [14] was conducted. The lift coefficient was 0.537 through this simulation, while the drag coefficient was 0.0045. XFOIL gave a lift coefficient error of 6.8 %

and a drag coefficient error of 14.2 % compared with the CFD one. The drag coefficient error was a little high but was relative to a very small quantity. In spite of that, in this case, the low-fidelity tool could predict the fluid dynamic performances correctly and quickly, as in the validation case. Figure 6 shows an isosurface at $Q = 50 \text{ s}^{-2}$ [20].

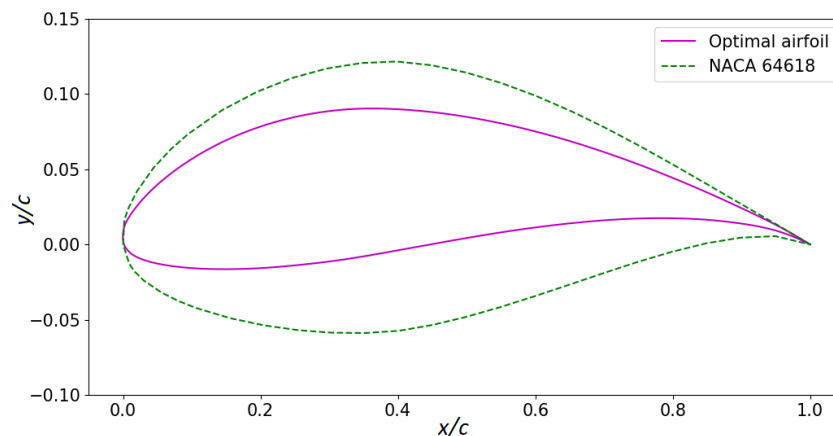


Figure 5. High-Reynolds optimal airfoil shape.

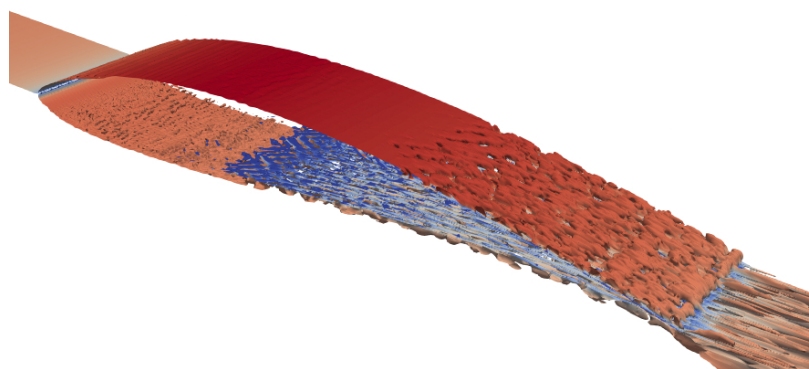


Figure 6. Isosurface at $Q = 50 \text{ s}^{-2}$ for the optimal high-Reynolds airfoil.

From this picture, it is possible to notice the turbulent separation on both sides of the airfoil. Due to the 3D features of the separation, it was not possible to evaluate the acoustic performances with a 2D simulation, so a 3D LES was performed. Regarding the noise emission, Figure 7 reported a comparison between the third-octave SPL trends for BPM and FWH analogy. As in the validation case, the SPL obtained with the FWH analogy was reported to the entire span using the correlation taken by [19]. Analyzing this graph, the OSPL was greatly influenced by the contribution related to the turbulent boundary layer on the suction side. At the higher frequency, instead, the most important contribution was due to the turbulent boundary layer on the pressure side. As in the high-Reynolds NACA 64618 case, the contributions related to the laminar vortex-shedding and angle of attack were negligible due to the high-Reynolds number and the slight angle of attack. From the curve of the SPL, it was possible to obtain an OSPL value of 61.2 dB_A , which was 1.3 dB lower than in the previous case. If the OSPL was calculated without the A-weighted correction, the OSPL for the optimal airfoil was 60.8 dB, while for the NACA 64618, it was equal to 63.0 dB. The corresponding noise reduction was 2.2 dB to be compared against 1.3 dB with the A-weighted correction.

The FWH analogy generally had the same trend as the BPM method, but at the lower frequency, the absolute value of the SPL was fairly higher than the BPM. Thanks to the A-weighted correction, despite the SPL value at the lower frequencies being higher than the BPM, the OSPL produced very similar results to the ones obtained with the low-fidelity tool. It is worth noting that both approaches also agree on capturing a maximum

value of the SPL at a frequency of around 2000 Hz. Overall, in this case, a satisfactory agreement between low- and high-fidelity tools was recorded for both aerodynamic and acoustics performances.

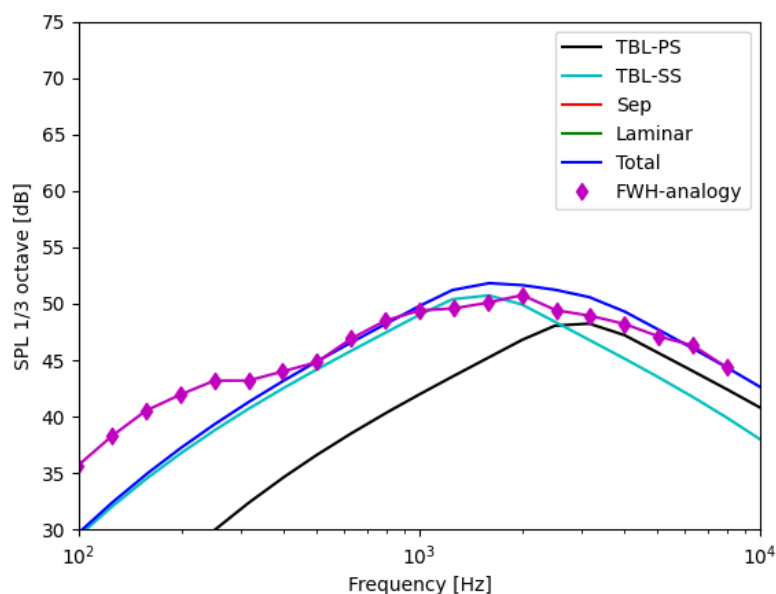


Figure 7. Comparison between BPM method and FWH analogy for the optimal high-Reynolds airfoil.

Table 1 reports a comparison between the acoustic and aerodynamic performances of the NACA 64618 airfoil and the optimal high-Reynolds airfoil. From this comparison, it is possible to notice how the optimal airfoil has a lower acoustic emission than the original one; moreover, it has a higher lift coefficient and a lower drag coefficient and, therefore a higher lift-to-drag ratio than the initial airfoil.

Table 1. Aerodynamic and acoustic comparison between NACA 64618 and optimal airfoil in the high-Reynolds regime.

Airfoil	AoA [°]	C_l	C_d	LDR	OSPL [dB _A]
NACA 64618	−0.268	0.52	0.0061	85.24	62.5
Optimal	−1.310	0.537	0.0045	119.3	61.2

3.3. NACA 64618 Low-Reynolds Number Case

The initial NACA 64618 airfoil with the same angle of attack as the high-Reynolds case was numerically tested with a chord-based Reynolds number of $2 \cdot 10^5$ in order to obtain a starting low-Reynolds number airfoil for the optimization process. With an angle of attack of -0.268° using the low-fidelity instrument, the lift coefficient was 0.4428. The resulting drag coefficient was 0.0165, and there was also a separation on the airfoil. The high-fidelity tool confirmed the presence of a separation and gave a lift coefficient of 0.465 and a drag coefficient of 0.0168. The low-fidelity tool in this case also underpredicted both coefficients by about 5 %, so it had a security advantage. The evolution of the flow over the airfoil obtained with the 3D LES simulation showed a mainly laminar separation; for this reason, in order to reduce the computational effort, a 2D LES simulation was used to predict the acoustic performance. The same structures were found in the 2D analysis, confirming the validity of the assumption.

The noise emitted by the interaction between the airfoil and the flow was lower than in the validation case, inasmuch as the velocity of the flow was about eight times lower. In fact, the OSPL obtained in the validation case, using the BPM method, was 62.5 dB_A, while the OSPL obtained, in this case, was 21.2 dB_A. Figure 8 reported the frequency spectrum for

the NACA 64618 in the low-Reynolds regime. The major contribution to the OSPL at the lower frequency was related to the laminar boundary layer, while at the higher frequency, it was due to the Turbulent boundary layer on the pressure side of the airfoil. The results obtained with the FWH analogy were reported in Figure 8; in particular, there was good agreement with the BPM result: only a slight SPL underprediction at the lower frequencies and overestimation at the medium frequencies were detected.

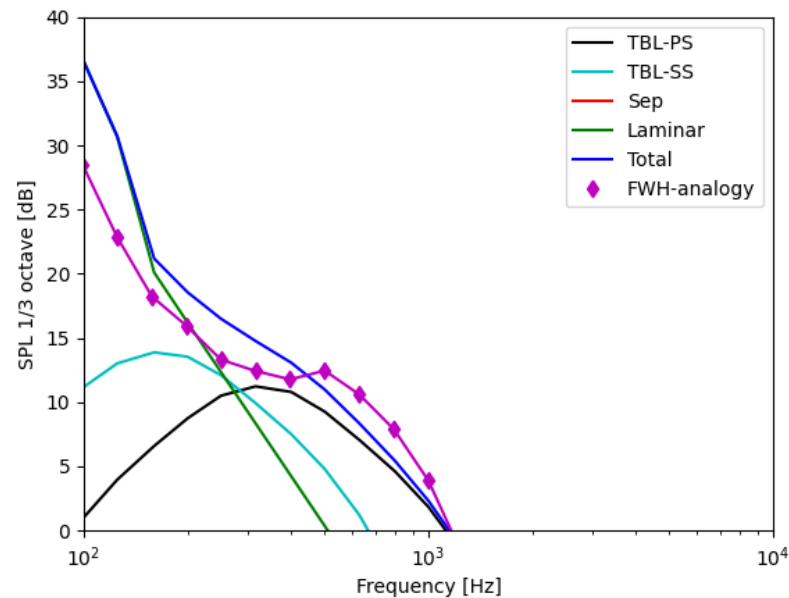


Figure 8. SPL 1/3 octave bands for low-Reynolds number NACA 64618.

3.4. Low-Reynolds Optimization

As in the high-Reynolds optimization subchapter, before the optimization process, the airfoil geometry parameters were changed one by one in order to understand the relationship between the individual geometrical features and the acoustic emission. From this analysis, the following conclusions have been found:

1. Thickness: Both T-PS and T-SS contributions had a higher value, and the maximum value was reached for a lower frequency. Instead, the Laminar contribution had a lower value and the frequency corresponding to the maximum value remains unchanged.
2. Position of maximum thickness: Similar effects as the thickness contribution.
3. Maximum camber value: The T-PS and T-SS contributions had a higher maximum value, but in this case, the frequencies at which these values were reached remain unchanged. As regards the laminar contribution, it had a lower value, and the frequency corresponding to the maximum value was lower.
4. Position of maximum camber: The same effects as the maximum camber contribution.

Since the highest contribution to the OSPL in the low-Reynolds regime was due to the laminar boundary layer, the optimal airfoil shape might have a higher thickness and a higher camber than the original NACA 64618. The optimization process, in accordance with the consideration just given, found a new airfoil with the following geometry parameters parameterized on the chord length c : (i) position of maximum thickness— $0.2c$, (ii) maximum thickness— $0.2c$, (iii) camber value— $0.045c$, and (iv) position of maximum camber— $0.5c$. Figure 9 reports a comparison between the original geometry and the optimized one for the low-Reynolds number regime, from which it is possible to notice how the new shape is more cambered and thicker than the NACA airfoil.

With the low-fidelity tool, the angle of attack that gave a lift coefficient equal to the low-Reynolds number case was -1.413° , while the drag coefficient was 0.0181. To validate the results, a CFD simulation was performed with an angle of attack of -1.413° . This resulted in a lift coefficient of 0.473 and a drag coefficient of 0.0196, which agrees with the

low-fidelity predictions. With this airfoil shape, both lift and drag coefficients were higher than in the low-Reynolds number NACA case, and the lift-to-drag ratio decreased by about 10 %. The structures on the suction side were mainly laminar, as shown in Figure 10, and the turbulent separation contribution could be neglected compared with the laminar one. Therefore, as in the baseline low-Reynolds number case, in order to speed up the computation, a 2D simulation for assessing aeroacoustics was performed.

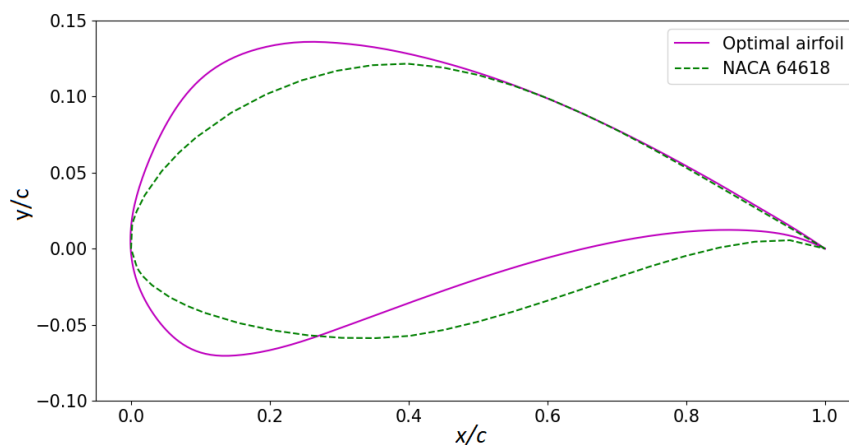


Figure 9. Low-Reynolds optimal airfoil shape.

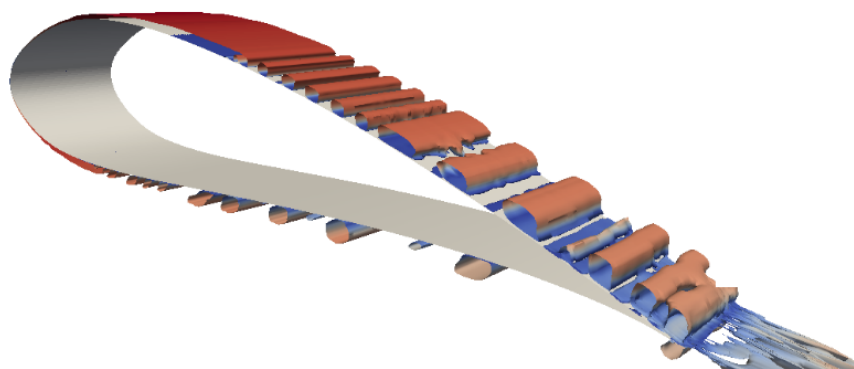


Figure 10. Isosurface at $Q = 50 \text{ s}^{-2}$ for the optimal low-Reynolds airfoil.

With the optimal airfoil, the OSPL obtained with the BPM method was 15.1 dB_A , while the relative frequency spectrum is shown in Figure 11. At the lower frequency, the major contribution to the SPL was due to the laminar boundary layer, while at the intermediate frequencies, the most important mechanism was the turbulent boundary layer on both the pressure and suction side.

The SPL was frequency-per-frequency lower than the low-Reynolds case, and the OSPL was 6 dB_A lower. The FWH analogy generally had a good agreement with the BPM data, as in the low-Reynolds number NACA 64618 case; only at the very low frequency was there an overestimation of the SPL. For this reason, the high-fidelity OSPL was very similar to the one obtained with the low-fidelity approach. It was worth noting that both approaches also agreed to capture a minimum in the spectrum around 200 Hz. The BPM model helped get insight into this, showing that the minimum was likely related to a sharp decrease in the laminar boundary layer effect at increasing frequencies. At the same time, the turbulent contribution on the suction side manifested as higher frequencies, and they were even higher for the pressure side. This frequency range between laminar and turbulent boundary layer contributions showed the minimum in SPL, confirmed by the FWH analysis.

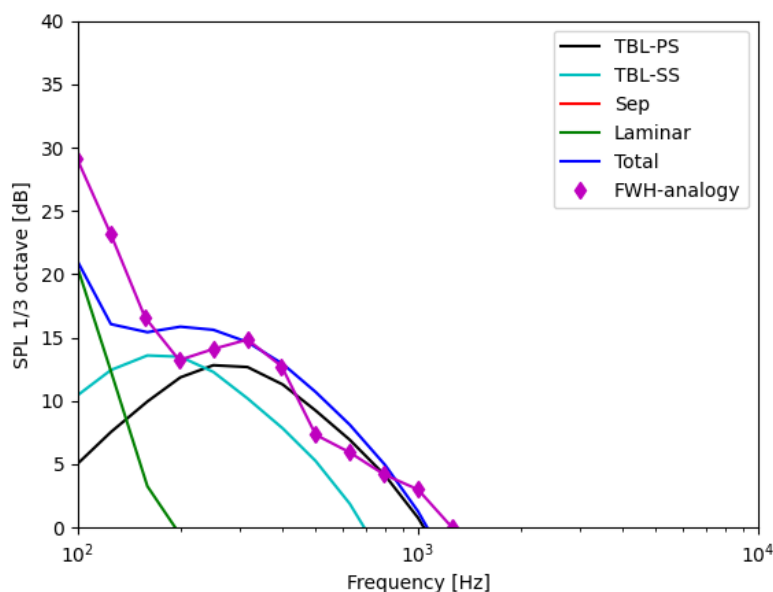


Figure 11. Sound pressure level 1/3 octave bands for the optimal low-Reynolds airfoil.

Table 2 reported a comparison between the acoustic and aerodynamic performances of the NACA 64618 airfoil and the optimal low-Reynolds airfoil. From this, it is possible to notice how the optimal airfoil has an important reduction in acoustic emission, a comparable lift-to-drag ratio, and a slightly higher lift coefficient than the original NACA 64168 airfoil.

Table 2. Aerodynamic and acoustic comparison between NACA 64618 and optimal airfoil in the low-Reynolds regime.

Airfoil	AoA [°]	C_l	C_d	LDR	OSPL [dB _A]
NACA 64618	−0.268	0.465	0.0168	27.6	21.2
Optimal	−1.413	0.473	0.0196	24.5	15.1

4. Conclusions

This work presented a general methodology that can be used to substitute the traditional airfoil that constitutes a blade of a fan in both low- and high-Reynolds regimes with silent ones that have comparable fluid dynamic performances but lower acoustic emissions. The selected starting airfoil does not represent all the possible applications but constitutes an optimization example. Therefore, a generic airfoil geometry can be used to initialize the process. In the first part of this elaboration, a noise spectra comparison between the BPM method (low-fidelity), FWH analogy (high-fidelity), and experimental data was evaluated for a high-Reynolds NACA 64618. The low- and high-fidelity results show good agreement, while the reference experimental data taken from [10] were about 5 dB lower, probably due to the presence of the Kevlar window, which enclosed the test section in the experimental setup. After the validation of both tools in the high-Reynolds regime, the BPM method was used in an SHGO optimizer to find the best airfoil shape with a lower acoustic emission in the frequency range typical of human hearing. The new airfoil had a noise reduction of about 1.3 dB than the original one; moreover, it had a higher lift coefficient and a lower drag coefficient and, therefore, a higher lift-to-drag ratio. The noise reduction reached is relevant because the NACA 64618 was developed to take into account acoustic emissions in the high-Reynolds regime. At this point, the original NACA airfoil with the same angle of attack as the high-Reynolds case was tested with a lower Reynolds number to validate the tools in the low-Reynolds regime. Also, both approaches gave approximately the same spectral SPL in this case. For this reason, the low-fidelity approach can be used for a good and quick estimation of the OSPL. Concerning the high-fidelity tool, it was demonstrated

that a 2D LES can capture the most relevant flow features connected to noise emission in such a regime. In the last part of the work, the same optimization process used for the high-Reynolds case was used to find the silent airfoil shape in such flow conditions. With this new geometry, a reduction of 6.1 dB is obtained; this improvement is greater than the previous optimization because the NACA 64618 is usually used in a high-Reynolds regime. Therefore, the starting point is not optimized for the acoustic emission or fluid dynamic performances with this flow condition. In addition, the aerodynamic performances of the optimal airfoil were comparable to the ones for the NACA 64618. For this reason, the optimal profile can directly replace the traditional NACA airfoil in a design procedure, as long as the angle of attack is changed. In particular, the high-Reynolds optimal geometry needs an AoA equal to -1.310° , while the low-Reynolds optimal airfoil needs an AoA equal to -1.413° with respect to the original AoA of -0.268° of the NACA 64618 airfoil. In future works, the effects of the stacking phase will be evaluated, and moreover, the effects of different mechanisms for noise suppression on a single airfoil will be taken into consideration.

Author Contributions: Conceptualization, N.C., M.P. (Mattia Piovan), E.F. and S.O.; methodology, N.C., M.P. (Mattia Piovan) and M.P. (Mattia Pinelli); formal analysis, M.P. (Mattia Piovan), N.C. and M.P. (Mattia Pinelli); investigation, N.C., M.P. (Mattia Piovan) and S.O.; writing—original draft preparation, M.P. (Mattia Piovan) and N.C.; writing—review and editing, M.P. (Mattia Piovan), N.C., M.P. (Mattia Pinelli), A.S., E.F. and S.O.; visualization, N.C. and M.P. (Mattia Piovan); supervision, M.P. (Mattia Pinelli) and A.S.; project administration, M.P. (Mattia Pinelli); resources, M.P. (Mattia Pinelli) and A.S. All authors have read and agreed to the published version of the manuscript.

Funding: This research received no external funding.

Institutional Review Board Statement: Not applicable.

Informed Consent Statement: Not applicable.

Data Availability Statement: Dataset available on request from the authors.

Conflicts of Interest: Author Nicola Casari was employed by the company ToffeeAM Ltd. The remaining authors declare that the research was conducted in the absence of any commercial or financial relationships that could be construed as a potential conflict of interest.

Abbreviations

The following abbreviations are used in this manuscript:

AoA	Angle of Attack
BEM	Boundary Element Method
BPM	Brooks Pope and Marcolini Method
c	Chord
CFL	Courant–Friedrichs–Lewy number
FWH	Ffowcs Williams Hawkins Analogy
LDR	Lift-to-Drag Ratio
LE	Leading Edge
OSPL	Overall Sound Pressure Level
PS	Pressure Side
SHG	Simplicial Homology Global
SPL	Sound Pressure Level
SS	Suction Side
TE	Trailing Edge

References

1. Qin, Y.; Tang, X.; Jia, T.; Duan, Z.; Zhang, J.; Li, Y.; Zheng, L. Noise and vibration suppression in hybrid electric vehicles: State of the art and challenges. *Renew. Sustain. Energy Rev.* **2020**, *124*, 109782. [[CrossRef](#)]
2. Rogers, A.L.; Manwell, J.F.; Wright, S. Wind turbine acoustic noise. In *Renewable Energy Research Laboratory*; University of Massachusetts: Amherst, MA, USA, 2006.
3. Wright, S. The acoustic spectrum of axial flow machines. *J. Sound Vib.* **1976**, *45*, 165–223. [[CrossRef](#)]

4. Moreau, S.; Roger, M. Competing broadband noise mechanisms in low-speed axial fans. *AIAA J.* **2007**, *45*, 48–57. [[CrossRef](#)]
5. Casari, N.; Fadiga, E.; Oliani, S.; Pinelli, M.; Piovan, M. A Low-Noise Airfoil for Low Reynolds Applications: A Multi-Fidelity Optimization. In Proceedings of the 15th European Turbomachinery Conference, Paper n. ETC2023-181, Budapest, Hungary, 24–28 April 2023. Available online: <https://www.euroturbo.eu/publications/proceedings-papers/etc2023-181/> (accessed on 1 July 2023).
6. Lacagnina, G.; Chaitanya, P.; Kim, J.H.; Berk, T.; Joseph, P.; Choi, K.S.; Ganapathisubramani, B.; Hasheminejad, S.M.; Chong, T.P.; Stalnov, O.; et al. Leading edge serrations for the reduction of aerofoil self-noise at low angle of attack, pre-stall and post-stall conditions. *Int. J. Aeroacoustics* **2021**, *20*, 130–156. [[CrossRef](#)]
7. Zhong, Y.; Li, Y.; Li, P.; Chen, J.; Xia, T.; Kuang, X. Blade Structure Design Based on Multi-objective Optimization of Automotive Fan. In *Proceedings of the Journal of Physics: Conference Series*; IOP Publishing: Bristol, UK, 2021; Volume 1952, p. 032022.
8. Ffowcs Williams, J.E.; Hawkings, D.L. Sound generation by turbulence and surfaces in arbitrary motion. *Philos. Trans. R. Soc. Lond. Ser. A Math. Phys. Sci.* **1969**, *264*, 321–342.
9. Brooks, T.F.; Pope, D.S.; Marcolini, M.A. *Airfoil Self-Noise and Prediction*; NASA Reference Publication 1208; National Technical Information Service: Springfield, VA, USA, 1989.
10. Shen, W.Z.; Zhu, W.J.; Fischer, A.; García, N.R.; Cheng, J.; Chen, J.; Madsen, J. Validation of the CQU-DTU-LN1 series of airfoils. In *Proceedings of the Journal of Physics: Conference Series*; IOP Publishing: Bristol, UK, 2014; Volume 555, p. 012093.
11. Casari, N.; Oliani, S.; Pinelli, M.; Piovan, M.; de Paola, E.; Stoica, L.G.; Marco, A.D.; Mollica, E. Towards a low-noise axial fan for automotive applications. *Proc. J. Phys. Conf. Ser.* **2022**, *2385*, 012137. [[CrossRef](#)]
12. Drela, M. XFOIL: An analysis and design system for low Reynolds number airfoils. In *Low Reynolds Number Aerodynamics*; Springer: Berlin/Heidelberg, Germany, 1989; pp. 1–12.
13. Nicoud, F.; Ducros, F. Subgrid-scale stress modelling based on the square of the velocity gradient tensor. *Flow Turbul. Combust.* **1999**, *62*, 183–200. [[CrossRef](#)]
14. Langtry, R.B.; Menter, F.R. Correlation-based transition modeling for unstructured parallelized computational fluid dynamics codes. *AIAA J.* **2009**, *47*, 2894–2906. [[CrossRef](#)]
15. Wagner, C.; Hüttl, T.; Sagaut, P. *Large-Eddy Simulation for Acoustics*; Cambridge University Press: Cambridge, UK, 2007; Volume 20.
16. Celik, I.B.; Cehreli, Z.N.; Yavuz, I. Index of Resolution Quality for Large Eddy Simulations. *J. Fluids Eng.* **2005**, *127*, 949–958.
17. Epikhin, A.; Evdokimov, I.; Kraposhin, M.; Kalugin, M.; Strijhak, S. Development of a dynamic library for computational aeroacoustics applications using the OpenFOAM open source package. *Procedia Comput. Sci.* **2015**, *66*, 150–157. [[CrossRef](#)]
18. Liang, Y.; Zhang, L.; Li, E.; Liu, X.; Yang, Y. Design considerations of rotor configuration for straight-bladed vertical axis wind turbines. *Adv. Mech. Eng.* **2014**, *2014*, 1–15. [[CrossRef](#)]
19. Abdessemed, C.; Bouferrouk, A.; Yao, Y. Aerodynamic and aeroacoustic analysis of a harmonically morphing airfoil using dynamic meshing. *Acoustics* **2021**, *3*, 177–199. [[CrossRef](#)]
20. Jeong, J.; Hussain, F. On the identification of a vortex. *J. Fluid Mech.* **1995**, *285*, 69–94. [[CrossRef](#)]

Disclaimer/Publisher’s Note: The statements, opinions and data contained in all publications are solely those of the individual author(s) and contributor(s) and not of MDPI and/or the editor(s). MDPI and/or the editor(s) disclaim responsibility for any injury to people or property resulting from any ideas, methods, instructions or products referred to in the content.